JOURNAL OF SPACECRAFT AND ROCKETS
Vol. 32, No. 1, January–February 1995

Analytical Solution and Parameter Estimation of Projectile Dynamics

Susanne Weiss* and Karl-Friedrich Doherr†
DLR, German Aerospace Research Establishment, D-38108 Braunschweig, Germany
and
Hartmut Schilling‡
Rheinmetall GmbH, D-40882 Ratingen, Germany

For the determination of the pitch, yaw, and roll characteristics of conventional projectiles an approach is presented that allows fast estimation of the projectile parameters from test data. To avoid numerical integration and the corresponding integration errors and convergence problems, an analytical solution of the six-degree-of-freedom differential equations of motion is introduced. Here, instead of time, the arc length of the flight path is taken as the independent variable. Also, linear aerodynamics without Magnus effects is assumed. The projectile parameters are determined by minimizing the squared sum of the differences between the measured and the simulated trajectory using a nongradient direct search method. As an example, yaw-card measurements from tests with KE rods (high-kinetic-energy projectiles) are analyzed. It is shown that the main aerodynamic coefficients can be extracted from these data. In addition, it is possible to identify the size and the location of the muzzle jump as well as the jump due to sabot separation.

Nomenclature

C_D	= drag coefficient
C_l, C_m, C_n	= coefficients of rolling, pitching, and yawing moment
C_X, C_Y, C_Z	= coefficients of longitudinal, lateral, and vertical force
D	= reference length (projectile diameter)
d	= damping factor
g	= acceleration due to gravity
I_x, I_q	= longitudinal and lateral moments of inertia
K_D	= reciprocal of the aerodynamic penetration
m	= projectile mass
p, q, r	= roll, pitch, and yaw rates
S	= reference area (projectile cross section)
s	= arc length along flight path (range)
s_D	= aerodynamic penetration
t	= time
u, v, w	= velocity components in body-fixed coordinates
V	= projectile velocity
x, y, z	= body-fixed coordinates
α_t	= effective angle of attack
ϵ	= factor of slenderness, $I_x/(2I_q)$
Φ, Θ, Ψ	= roll, pitch, and yaw angles
ρ	= density of air

Subscripts

0	= initial value
g	= earth-fixed
m	= muzzle jump
s	= jump due to sabot separation

Superscript

$'$	= derivative with respect to arc length (range)

Received June 17, 1993; presented as Paper 93-3637 at the AIAA Atmospheric Flight Mechanics Conference, Monterey, CA, Aug. 9–11, 1993; revision received Feb. 14, 1994; accepted for publication Feb. 15, 1994.

*Research Scientist, Institute of Flight Mechanics. Member AIAA.
†Head, Mathematical Methods and Data Handling Branch, Institute of Flight Mechanics. Member AIAA.
‡Head, System Simulation Department, Institute of Flight Mechanics. Member AIAA.

Introduction

DURING the development of new ammunition the aerodynamic parameters must be estimated first on the basis of existing experience, design data, and wind-tunnel results. Later, for conventional ammunition such as KE rods (high-kinetic-energy rods) or explosively formed projectiles flying in the high-Mach-number regime, many field tests are usually needed to prove the required hit accuracy and lethality. These tests provide an opportunity for the aerodynamicist to leave the simulation-only status of the development phase and to extract and to verify the aerodynamic parameters of the tested configurations from the recorded trajectory data.

To observe the trajectories, a common test method is to place a number of yaw cards perpendicular to the flight path (Fig. 1). From the trace that a projectile leaves on the paper cards it is possible to extract information about the roll, yaw, and pitch attitude and about the deviations of the projectile path from the centerline. Additional data from separate measurements provide initial position and velocity as well as the velocity decay.

Beside yaw cards, there are other measurement techniques for documenting projectile motion in ballistic test ranges, which are fundamentally photographic in concept and which have the great advantage of not disturbing the observed phenomena. Moreover, they can provide a visualization of the projectiles and even of the flowfield at a number of stations along the trajectory. However, the use of yaw cards is much simpler and less costly and is therefore preferred when repeated tests of various configurations and shapes are to be made.

For the analysis of the experimental data different methods exist.[1–5] Recently a study was made by Rheinmetall GmbH and by the Institute of Flight Mechanics of DLR to apply existing system identification experience[6–11] to estimate the dynamic parameters of projectiles from yaw-card data.

A mathematical method and the related computer program were developed allowing the determination of the aerodynamic coefficients, damping derivatives, and initial disturbances due to muzzle jump and sabot separation. The initial disturbances occur at and shortly behind the muzzle and therefore before the first yaw card is penetrated. Since no measured data are available between the muzzle and the first yaw card, the usual approach of using a numerical

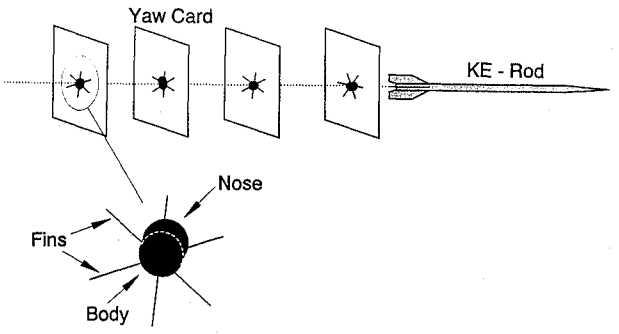

Fig. 1 Yaw-card experiment.

integration scheme in the estimation procedure is not feasible. The integration errors as well as the lack of trajectory information outside the range of the yaw cards would cause severe convergence problems, making the estimation of initial disturbances impossible. This problem stimulated the development of an analytical solution of the differential equations and its inclusion in the projectile parameter estimation algorithm.

To determine the projectile parameters a maximum-likelihood cost function and a nongradient optimization method[12] are used. The corresponding computer program allows quick analysis and visualization of the measured data.

General Analytical Solution

In 1990, Bockemüller and Weiss[13] developed a closed solution of the nonlinear six-degree-of-freedom (6-DOF) equations of motion for slender bodies ($I_x/I_q \approx 0$). There, instead of time, the arc length along the flight path was taken as the independent variable. The motion perpendicular to the flight path (yaw and pitch) is separated from the motion along and about the flight path (velocity and roll). The aerodynamics of the configuration is assumed to be linear, and Magnus forces are neglected. These limitations are not serious for fin-stabilized projectiles on the short ranges of typical field tests, when the projectiles do not develop large angles of attack or very high roll rates. In the following, this solution is expanded to the practical case $I_x/I_q \neq 0$. As Fig. 2 shows, this term causes a rotation of the pitch-yaw pendulum plane.

Differential Equations

The motion of bodies with rotational symmetry is fully described by the following system of differential equations:

Velocity Components

$$\dot{u} = (\rho/2)V^2(S/m)C_X + vr - wq - g\sin\Theta \tag{1a}$$

$$\dot{v} = (\rho/2)V^2(S/m)C_Y + wp - ur + g\sin\Phi\cos\Theta \tag{1b}$$

$$\dot{w} = (\rho/2)V^2(S/m)C_Z + uq - vp + g\cos\Phi\cos\Theta \tag{1c}$$

Angular Rates:

$$\dot{p} = (\rho/2)V^2(SD/I_x)C_l \tag{2a}$$

$$\dot{q} = (\rho/2)V^2(SD/I_q)C_m + (1 - (I_x/I_q))pr \tag{2b}$$

$$\dot{r} = (\rho/2)V^2(SD/I_q)C_n - (1 - (I_x/I_q))pq \tag{2c}$$

Euler Angles:

$$\dot{\Phi} = p + q\sin\Phi\tan\Theta + r\cos\Phi\tan\Theta \tag{3a}$$

$$\dot{\Theta} = q\cos\Phi - r\sin\Phi \tag{3b}$$

$$\dot{\Psi} = \frac{q\sin\Phi}{\cos\Theta} + \frac{r\cos\Phi}{\cos\Theta} \tag{3c}$$

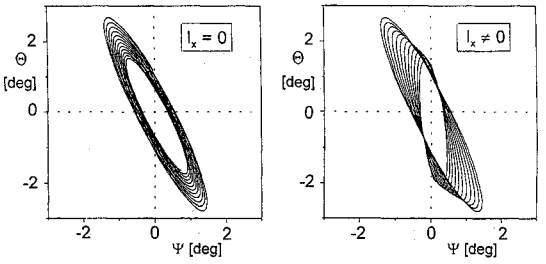

Fig. 2 Influence of longitudinal moment of inertia on the rotation of the plane of oscillation.

Position in Earth-Fixed Coordinates:

$$\dot{x}_g = u\cos\Theta\cos\Psi + v(\sin\Phi\sin\Theta\cos\Psi - \cos\Phi\sin\Psi) + w(\cos\Phi\sin\Theta\cos\Psi + \sin\Phi\sin\Psi) \tag{4a}$$

$$\dot{y}_g = u\cos\Theta\sin\Psi + v(\sin\Phi\sin\Theta\sin\Psi + \cos\Phi\cos\Psi) + w(\cos\Phi\sin\Theta\sin\Psi - \sin\Phi\cos\Psi) \tag{4b}$$

$$\dot{z}_g = -u\sin\Theta + v\sin\Phi\cos\Theta + w\cos\Phi\cos\Theta \tag{4c}$$

Aerodynamic Model

For small disturbances only, the aerodynamics can be assumed to be linear in the effective angle of attack α_t, which is the polar angle between the airflow and the longitudinal axis of the projectile: for $w_t = \sqrt{v^2 + w^2}$,

$$\alpha_t = |\arctan(w_t/u)| \tag{5}$$

Furthermore, neglecting Magnus forces leads to the following force and moment coefficients:

$$C_X = C_{X0} \tag{6a}$$

$$C_Y = C_{Z\alpha}\alpha_t(v/w_t) \tag{6b}$$

$$C_Z = C_{Z\alpha}\alpha_t(w/w_t) \tag{6c}$$

and

$$C_l = C_{l0} + C_{lp}p(D/2V) \tag{7a}$$

$$C_m = C_{m\alpha}\alpha_t(w/w_t) + C_{mq}q(D/2V) \tag{7b}$$

$$C_n = -C_{m\alpha}\alpha_t(v/w_t) + C_{mq}r(D/2V) \tag{7c}$$

Translation and Rotation

Because of the high longitudinal velocity and comparably small yawing and pitch motion of the projectile, the motion along and about the flight path (velocity and roll) can be separated from the motion perpendicular to the flight path (yaw and pitch).

Velocity

Also, the influence of gravity, yawing motion, and pitching motion on the deceleration of the projectile can be neglected. Therefore, Eq. (1a) can be replaced (where $C_D = -C_{X0}$) by

$$\dot{V} = -(\rho/2)V^2(S/m)C_D \tag{8}$$

Substituting arc length s for time t as the independent variable results in

$$\frac{\mathrm{d}}{\mathrm{d}t}(\cdots) = \frac{\mathrm{d}}{\mathrm{d}s}(\cdots)\frac{\mathrm{d}s}{\mathrm{d}t} = \frac{\mathrm{d}}{\mathrm{d}s}(\cdots)V \tag{9}$$

Equation (8) can be reformulated as

$$\frac{\mathrm{d}V}{\mathrm{d}s} = -\frac{\rho}{2}\frac{S}{m}C_D V, \qquad V(0) = V_0 \tag{10}$$

which has the solution where $K_D = (\rho/2)(S/m)C_D$

$$V(s) = V_0 e^{-K_D s} \tag{11}$$

Here, K_D is the reciprocal of the aerodynamic penetration s_D defined by Larabee,[14] and s_D is the distance an object travels until its speed is reduced by a factor of $1/e$ by drag proportional to the square of the speed.

Roll Rate

Formulating the differential equation (2a) for the roll rate also with respect to arc length via Eq. (9) and using Eq. (7a) leads to

$$\frac{\mathrm{d}p}{\mathrm{d}s} = \frac{\rho}{2}\frac{SD}{I_x}C_{l0}V + \frac{\rho}{2}\frac{SD^2}{2I_x}C_{lp}p, \qquad p(0) = p_0 \tag{12}$$

which has the solution

$$p(s) = \frac{K_{l0}\,V_0}{K_{lp}+K_D}\left(e^{K_{lp}s} - e^{-K_D s}\right) + p_0 e^{K_{lp}s} \tag{13}$$

where

$$K_{l0} = \frac{\rho}{2}\frac{SD}{I_x}C_{l0} \quad \text{and} \quad K_{lp} = \frac{\rho}{2}\frac{SD^2}{2I_x}C_{lp} \tag{14}$$

Roll Attitude

Taking into account that the pitch attitude for horizontal flight is small and that the roll rate, once it is built up, is much higher than the pitch and yaw rates, Eq. (3a) for the roll angle can be simplified to

$$\dot{\Phi} = p \tag{15}$$

Formulating this equation with respect to arc length [Eq. (9)] and substituting the solutions for roll rate and velocity, Eqs. (11) and (13), yields

$$\frac{\mathrm{d}\Phi}{\mathrm{d}s} = \frac{K_{l0}}{K_{lp}+K_D}\left(e^{(K_{lp}+K_D)s} - 1\right) + \frac{p_0}{V_0}e^{(K_{lp}+K_D)s} \tag{16}$$

Because of the rotational symmetry of the projectile, the body-fixed coordinate system can be chosen so that $\Phi(0) = 0$, which leads to

$$\Phi(s) = \frac{K_{l0}}{(K_{lp}+K_D)^2}\left(e^{(K_{lp}+K_D)s} - (K_{lp}+K_D)s - 1\right) + \frac{p_0}{V_0}\frac{1}{K_{lp}+K_D}\left(e^{(K_{lp}+K_D)s} - 1\right) \tag{17}$$

for the roll angle.

Lateral Velocities and Angular Rates

The yawing and pitching motion perpendicular to the flight path is a pendulum (coning) motion that is caused by initial disturbances such as the muzzle jump. The influence of gravity on this oscillation can be neglected. Furthermore, setting $u \approx V$ and inserting Eqs. (6b), (6c), (7b), and (7c) into the corresponding Eqs. (1b), (1c), (2b), and (2c) leads to

$$\dot{v} = \frac{\rho}{2}V^2\frac{S}{m}C_{Z\alpha}\alpha_t\frac{v}{w_t} + wp - Vr \tag{18a}$$

$$\dot{w} = \frac{\rho}{2}V^2\frac{S}{m}C_{Z\alpha}\alpha_t\frac{w}{w_t} + Vq - vp \tag{18b}$$

$$\dot{q} = \frac{\rho}{2}V^2\frac{SD}{I_q}\left(C_{m\alpha}\alpha_t\frac{w}{w_t} + C_{mq}q\frac{D}{2V}\right) + pr\left(1 - \frac{I_x}{I_q}\right) \tag{18c}$$

$$\dot{r} = \frac{\rho}{2}V^2\frac{SD}{I_q}\left(-C_{m\alpha}\alpha_t\frac{v}{w_t} + C_{mq}r\frac{D}{2V}\right) - pq\left(1 - \frac{I_x}{I_q}\right) \tag{18d}$$

for the lateral velocity components and pitch and yaw rate. For small effective angle of attack ($\alpha_t < 5\,\mathrm{deg}$),

$$\alpha_t \approx \tan\alpha_t = \left|\frac{w_t}{u}\right| \approx \frac{w_t}{V} \tag{19}$$

The differential equations with respect to arc length are

$$\frac{\mathrm{d}v}{\mathrm{d}s} = K_{Z\alpha}v + \frac{p}{V}w - r \tag{20a}$$

$$\frac{\mathrm{d}w}{\mathrm{d}s} = -\frac{p}{V}v + K_{Z\alpha}w + q \tag{20b}$$

$$\frac{\mathrm{d}q}{\mathrm{d}s} = K_{m\alpha}w + K_{mq}q + \frac{p}{V}\left(1 - \frac{I_x}{I_q}\right)r \tag{20c}$$

$$\frac{\mathrm{d}r}{\mathrm{d}s} = -K_{m\alpha}v - \frac{p}{V}\left(1 - \frac{I_x}{I_q}\right)q + K_{mq}r \tag{20d}$$

where

$$K_{Z\alpha} = \frac{\rho}{2}\frac{S}{m}C_{Z\alpha}, \quad K_{m\alpha} = \frac{\rho}{2}\frac{SD}{I_q}C_{m\alpha}, \quad K_{mq} = \frac{\rho}{2}\frac{SD^2}{2I_q}C_{mq} \tag{21}$$

From Ref. 13 it is known that the resulting oscillation has a damping factor of

$$d = (K_{Z\alpha} + K_{mq})/2 \tag{22}$$

and that the plane of oscillation is slowly rotating when the longitudinal moment of inertia I_x cannot be neglected against I_q. This motivates the following substitution:

$$\hat{v} = e^{-ds}\{v\cos[(1-\epsilon)\Phi] - w\sin[(1-\epsilon)\Phi]\} \tag{23a}$$

$$\hat{w} = e^{-ds}\{v\sin[(1-\epsilon)\Phi] + w\cos[(1-\epsilon)\Phi]\} \tag{23b}$$

$$\hat{q} = e^{-ds}\{q\cos[(1-\epsilon)\Phi] - r\sin[(1-\epsilon)\Phi]\} \tag{23c}$$

$$\hat{r} = e^{-ds}\{q\sin[(1-\epsilon)\Phi] + r\cos[(1-\epsilon)\Phi]\} \tag{23d}$$

where

$$\epsilon = I_x/(2I_q) \tag{24}$$

The differential equations for the new set of variables are

$$\hat{v}' = k\hat{v} + \epsilon\Phi'\hat{w} - \hat{r} \tag{25a}$$

$$\hat{w}' = -\epsilon\Phi'\hat{v} + k\hat{w} + \hat{q} \tag{25b}$$

$$\hat{q}' = K_{m\alpha}\hat{w} - k\hat{q} - \epsilon\Phi'\hat{r} \tag{25c}$$

$$\hat{r}' = -K_{m\alpha}\hat{v} + \epsilon\Phi'\hat{q} - k\hat{r} \tag{25d}$$

where

$$k = (K_{Z\alpha} - K_{mq})/2 \tag{26}$$

Calculating second derivatives with respect to arc length allows separation of the translational velocities from the angular rates:

$$\hat{v}'' + \omega^2\hat{v} = -\epsilon^2(\Phi')^2\hat{v} + \epsilon(\Phi'' + 2k\Phi')\hat{w} \tag{27a}$$

$$\hat{w}'' + \omega^2\hat{w} = -\epsilon^2(\Phi')^2\hat{w} - \epsilon(\Phi'' + 2k\Phi')\hat{v} \tag{27b}$$

$$\hat{q}'' + \omega^2\hat{q} = -\epsilon^2(\Phi')^2\hat{q} - \epsilon(\Phi'' + 2k\Phi')\hat{r} \tag{27c}$$

$$\hat{r}'' + \omega^2\hat{r} = -\epsilon^2(\Phi')^2\hat{r} + \epsilon(\Phi'' + 2k\Phi')\hat{q} \tag{27d}$$

where

$$\omega^2 = -\left(k^2 + K_{m\alpha}\right) \tag{28}$$

Because ϵ, Φ'' and k are small, all terms on the right-hand sides of Eqs. (27) are small of higher order and can therefore be neglected. This is equivalent to neglecting all $\epsilon\Phi'$ terms in the differential

equations (25) and leads to simple sinusoidal solutions with frequency ω for the substituted variables $\hat{v}$, $\hat{w}$, $\hat{q}$, and $\hat{r}$.

The solutions for these variables can have only four independent integration constants. These are determined by inserting the sinusoidal solutions into the differential equations (25), which leads to

$$\hat{v} = A\cos(\omega s + \sigma_1) + B\cos(\omega s + \sigma_2) \tag{29a}$$

$$\hat{w} = A\sin(\omega s + \sigma_1) - B\sin(\omega s + \sigma_2) \tag{29b}$$

$$\hat{q} = -K_1[A\sin(\omega s + \sigma_1 - \varphi) - B\sin(\omega s + \sigma_2 - \varphi)] \tag{29c}$$

$$\hat{r} = K_1[A\cos(\omega s + \sigma_1 - \varphi) + B\cos(\omega s + \sigma_2 - \varphi)] \tag{29d}$$

where

$$\varphi = \arctan(\omega/k) \quad \text{and} \quad K_1 = \sqrt{-K_{m\alpha}} \tag{30}$$

Inverting the substitution [Eqs. (23)] finally leads to

$$v(s) = e^{ds}\{A\cos[\omega s - (1-\epsilon)\Phi + \sigma_1] + B\cos[\omega s + (1-\epsilon)\Phi + \sigma_2]\} \tag{31a}$$

$$w(s) = e^{ds}\{A\sin[\omega s - (1-\epsilon)\Phi + \sigma_1] - B\sin[\omega s + (1-\epsilon)\Phi + \sigma_2]\} \tag{31b}$$

$$q(s) = -K_1 e^{ds}\{A\sin[\omega s - (1-\epsilon)\Phi + \sigma_1 - \varphi] - B\sin[\omega s + (1-\epsilon)\Phi + \sigma_2 - \varphi]\} \tag{31c}$$

$$r(s) = K_1 e^{ds}\{A\cos[\omega s - (1-\epsilon)\Phi + \sigma_1 - \varphi] + B\cos[\omega s + (1-\epsilon)\Phi + \sigma_2 - \varphi]\} \tag{31d}$$

The parameters A, B, σ_1, and σ_2 are determined from the initial conditions via

$$A^2 = \frac{(k^2+\omega^2)x_{10} + x_{20} + 2kx_{30} + 2\omega x_{40}}{4\omega^2} \tag{32a}$$

$$B^2 = \frac{(k^2+\omega^2)x_{10} + x_{20} + 2kx_{30} + 2\omega x_{40}}{4\omega^2} \tag{32b}$$

$$\tan(\sigma_1 + \sigma_2) = \frac{2k\omega x_{10} + 2\omega x_{30}}{(k^2+\omega^2)x_{10} + x_{20} + 2kx_{30}} \tag{32c}$$

$$\tan(\sigma_1 - \sigma_2) = \frac{2v_0w_0\left[(k^2+\omega^2)x_{10} - x_{20}\right] - 2(w_0r_0 - v_0q_0)[kx_{10} + x_{30}]}{\left(v_0^2 - w_0^2\right)\left[(k^2+\omega^2)x_{10} - x_{20}\right] - 2(v_0r_0 + w_0q_0)(kx_{10} + x_{30})} \tag{32d}$$

where

$$x_{10} = v_0^2 + w_0^2 \tag{33a}$$

$$x_{20} = q_0^2 + r_0^2 \tag{33b}$$

$$x_{30} = w_0q_0 - v_0r_0 \tag{33c}$$

$$x_{40} = v_0q_0 + w_0r_0 \tag{33d}$$

Attitude Angles and Positions

Because pitch and yaw angles are assumed to be small, the assumptions

$$\cos\Theta \approx 1, \quad \cos\Psi \approx 1, \quad \sin\Theta \approx \Theta, \quad \sin\Psi \approx \Psi, \quad \sin\Theta\sin\Psi \approx 0 \tag{34}$$

are valid. With $u \approx V$, Eqs. (3b), (3c), (4b), and (4c) are transformed into

$$\dot{\Theta} = q\cos\Phi - r\sin\Phi \tag{35a}$$

$$\dot{\Psi} = q\sin\Phi + r\cos\Phi \tag{35b}$$

$$\dot{y}_g = V\Psi + v\cos\Phi - w\sin\Phi \tag{35c}$$

$$\dot{z}_g = -V\Theta + v\sin\Phi + w\cos\Phi \tag{35d}$$

or, with respect to arc length,

$$\frac{d\Theta}{ds} = \frac{q}{V}\cos\Phi - \frac{r}{V}\sin\Phi \tag{36a}$$

$$\frac{d\Psi}{ds} = \frac{q}{V}\sin\Phi + \frac{r}{V}\cos\Phi \tag{36b}$$

$$\frac{dy_g}{ds} = \Psi + \frac{v}{V}\cos\Phi - \frac{w}{V}\sin\Phi \tag{36c}$$

$$\frac{dz_g}{ds} = -\Theta + \frac{v}{V}\sin\Phi + \frac{w}{V}\cos\Phi \tag{36d}$$

Substituting the solutions for q, r, and V, Eqs. (31) and (11), first leads to

$$\frac{d\Theta}{ds} = -\frac{K_1}{V_0}e^{d_1 s}[A\sin(\omega s + \epsilon\Phi + \sigma_1 - \varphi) - B\sin(\omega s - \epsilon\Phi + \sigma_2 - \varphi)] \tag{37a}$$

$$\frac{d\Psi}{ds} = \frac{K_1}{V_0}e^{d_1 s}[A\cos(\omega s + \epsilon\Phi + \sigma_1 - \varphi) + B\cos(\omega s - \epsilon\Phi + \sigma_2 - \varphi)] \tag{37b}$$

where

$$d_1 = K_D + d \tag{38}$$

Within the argument of the sin and cos functions, the term $\varepsilon\Phi$, which causes the rotation of the plane of oscillation, varies only very slowly compared to ωs. It can therefore be assumed a constant for the integration. This then leads to

$$\Theta(s) = K_2 e^{d_1 s}[A\cos(\omega s + \epsilon\Phi + \sigma_1 - \varphi - \eta) + B\cos(\omega s - \epsilon\Phi + \sigma_2 - \varphi - \eta)] + C_\Theta \tag{39a}$$

$$\Psi(s) = K_2 e^{d_1 s}[A\sin(\omega s + \epsilon\Phi + \sigma_1 - \varphi - \eta) - B\sin(\omega s - \epsilon\Phi + \sigma_2 - \varphi - \eta)] + C_\Psi \tag{39b}$$

where

$$K_2 = \frac{1}{V_0}\sqrt{\frac{-K_{m\alpha}}{(K_D+d)^2 + \omega^2}} \quad \text{and} \quad \eta = \arctan\frac{\omega}{K_D + d} \tag{40}$$

The constants C_Θ and C_Ψ are defined by the initial conditions $\Theta(0)$ and $\Psi(0)$.

Substituting these results into the differential equations (30) for the positions then yields

$$\frac{dy_g}{ds} = K_3 e^{d_1 s}[A\cos(\omega s + \epsilon\Phi + \sigma_1 - \eta) + B\cos(\omega s - \epsilon\Phi + \sigma_2 - \eta)] + C_\Psi \tag{41a}$$

$$\frac{dz_g}{ds} = K_3 e^{d_1 s}[A\sin(\omega s + \epsilon\Phi + \sigma_1 - \eta) - B\sin(\omega s - \epsilon\Phi + \sigma_2 - \eta)] - C_\Theta \tag{41b}$$

where

$$K_3 = \frac{1}{V_0}\frac{K_D + K_{Z\alpha}}{\sqrt{(K_D+d)^2 + \omega^2}} \tag{42}$$

A similar approximate integration leads to

$$y_g(s) = K_4 e^{d_1 s}[A\cos(\omega s + \epsilon\Phi + \sigma_1 - \varphi - \eta) + B\cos(\omega s - \epsilon\Phi + \sigma_2 - \varphi - \eta)] + C_\Psi s + C_y \quad (43a)$$

$$z_g(s) = K_4\, e^{d_1 s}[A\sin(\omega s + \epsilon\Phi + \sigma_1 - \varphi - \eta) - B\sin(\omega s - \epsilon\Phi + \sigma_2 - \varphi - \eta)] - C_\Theta s + C_z \quad (43b)$$

where

$$K_4 = \frac{1}{V_0}\frac{K_D + K_{Z\alpha}}{(K_D + d)^2 + \omega^2} \quad (44)$$

The constants C_y and C_z are again determined by the initial conditions.

Taking Gravity into Account

While solving the differential equations for the oscillation, gravity has been neglected. The influence of gravity on the z coordinate can, as is often done in ballistics, be taken into account by simply adding the term $gt^2/2$ to the solution already found. The time t follows from Eqs. (9) and (11):

$$t = \int_0^t \mathrm{d}t' = \int_0^s V(s')\,\mathrm{d}s' = \int_0^s e^{K_D s'}\mathrm{d}s' = \frac{1}{V_0 K_D}(e^{K_D s} - 1) \quad (45)$$

Therefore

$$\tfrac{1}{2}gt^2 = \frac{g}{2K_D^2 V_0^2}(e^{2K_D s} - 2e^{K_D s} + 1) \quad (46)$$

has to be added to the solution [Eq. (43)] for z_g.

In a similar way, the influence of gravity on the pitch angle can be taken into account. Gravity adds a term of

$$-g\frac{\cos\Theta}{V} \approx -\frac{g}{V} \quad (47)$$

to $\mathrm{d}\Theta/\mathrm{d}t$, or of $-g/V^2$ to $\mathrm{d}\Theta/\mathrm{d}s$. Therefore

$$-\int_0^s \frac{g}{V^2}\mathrm{d}s' = \frac{-g}{V_0^2}\int_0^s e^{2K_D s'}\mathrm{d}s' = \frac{-g}{2V_0^2 K_D}(e^{2K_D s} - 1) \quad (48)$$

has to be added to the solution [Eq. (39)] for the pitch angle Θ.

Comparison with 6-DOF Simulation

To illustrate the quality of the analytical solution derived above, the motion of a projectile with $I_x/I_q = 0.009$ flying at Mach 3 was simulated. The projectile parameters and the initial conditions are given in Table 1. Figure 3 shows that the match between the 6-DOF simulation and the analytical solution is very good in all variables over the whole simulation distance of 1000 m. Figure 4 demonstrates that the rotation of the plane of oscillation and the influence of gravity on the pitch angle are modeled with sufficient accuracy.

Table 1 Data for the 6-DOF simulation

Missile parameters	
$D = 0.072$ m	$I_x = 0.0076$ kg-m^2
$m = 13.1$ kg	$I_q = 0.84$ kg-m^2
Initial conditions	
$V_0 = 1000$ m/s	$p_0 = 0.0$ rad/s
$v_0 = 5.87$ m/s	$q_0 = 0.341$ rad/s
$w_0 = -5.48$ m/s	$r_0 = -0.246$ rad/s
Derivatives	
$C_D = 1.08$	
$C_{l0} = 0.00741$	$C_{lp} = -0.46$
$C_{Z\alpha} = 6.23$	
$C_{m\alpha} = -5.23$	$C_{mq} = -639.0$

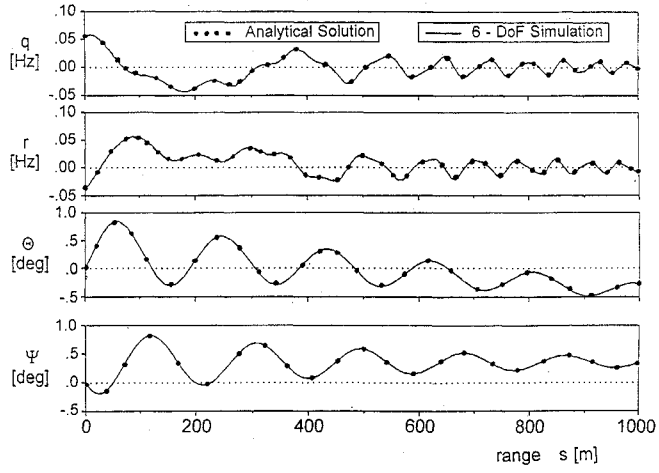

Fig. 3 Comparison of analytical and numerical solution of 6-DOF equations of motion.

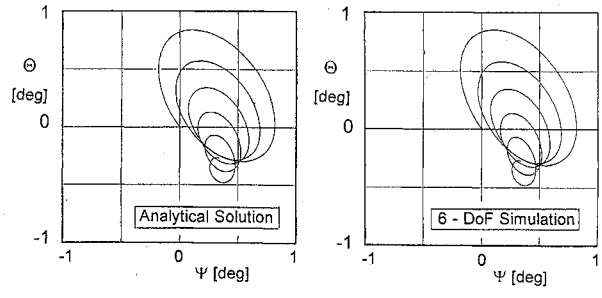

Fig. 4 Pitch angle vs yaw angle (analytical and numerical solution).

Impulse-Initiated Pendulum Motion of KE Rods

The analytical solutions derived above are applied next to estimate the parameters of KE rods. These usually suffer two disturbances: 1) the muzzle jump due to the motion of the gun muzzle when the projectile leaves the barrel, and 2) the aerodynamic impulse due to separation of the sabot. The latter takes place along the first few meters of the flight path. An additional impulse is induced if asymmetric separation of the sabot occurs, which will almost always be the case.[15–18]

Initial Disturbance Due to Muzzle Jump

If the initial disturbance is caused by an impulse that occurs at a distance Δx behind the projectile center of gravity, the following relation between the initial velocities and angular rates is valid:

$$I_q\begin{pmatrix} q_0 \\ r_0 \end{pmatrix} = \Delta x m\begin{pmatrix} w_0 \\ -v_0 \end{pmatrix} \quad (49)$$

such that

$$v_0 = -\lambda r_0, \quad w_0 = \lambda q_0 \quad \text{with} \quad \lambda = \frac{I_q}{\Delta x\, m} \quad (50)$$

Substituting this into the equations (32) leads to the following relations between A, B, σ_1, and σ_2:

$$A = B, \quad \sigma_2 = \sigma_1 - 2\theta \quad \text{with} \quad \theta = \arctan\frac{w_0}{v_0} \quad (51)$$

Setting

$$\sigma_a = (\sigma_1 + \sigma_2)/2 \quad \text{and} \quad \sigma_b = (\sigma_1 - \sigma_2)/2 \quad (52)$$

simplifies the solutions to

$$v(s) = 2Ae^{ds}\cos(\omega s + \sigma_a)\cos[(1-\epsilon)\Phi - \sigma_b] \quad (53a)$$

$$w(s) = 2Ae^{ds}\cos(\omega s + \sigma_a)\sin[(1-\epsilon)\Phi - \sigma_b] \quad (53b)$$

$$q(s) = 2AK_1 e^{ds}\cos(\omega s + \sigma_a - \phi)\sin[(1-\epsilon)\Phi - \sigma_b] \quad (53c)$$

$$r(s) = 2AK_1 e^{ds}\cos(\omega s + \sigma_a - \phi)\cos[(1-\epsilon)\Phi - \sigma_b] \quad (53d)$$

for the velocities and rates, and to

$$\Theta(s) = -2AK_2 e^{d_1 s}\cos(\omega s + \sigma_a - \varphi - \eta) \times \sin(\epsilon\Phi + \sigma_b) + C_\Theta \tag{54a}$$

$$\Psi(s) = 2AK_2 e^{d_1 s}\cos(\omega s + \sigma_a - \varphi - \eta) \times \cos(\epsilon\Phi + \sigma_b) + C_\Psi \tag{54b}$$

$$y_g(s) = 2AK_4 e^{d_1 s}\cos(\omega s + \sigma_a - 2\eta) \times \cos(\epsilon\Phi + \sigma_b) + C_\Psi s + C_y \tag{54c}$$

$$z_g(s) = 2AK_4 e^{d_1 s}\cos(\omega s + \sigma_a - 2\eta) \times \sin(\epsilon\Phi + \sigma_b) + C_\Theta s + C_z \tag{54d}$$

for the attitudes and positions. The influence of gravity on pitch angle and vertical position has to be added as described previously.

The constants σ_a, σ_b, and A are determined by

$$\sigma_a = \arctan\left(\frac{1/\lambda - k}{\omega}\right) \tag{55a}$$

$$\sigma_b = \arctan\frac{w_0}{v_0} = \arctan\frac{-q_0}{r_0} \tag{55b}$$

$$A = \frac{\sqrt{v_0^2 + w_0^2}}{2\cos\sigma_a} = \frac{\sqrt{q_0^2 + r_0^2}}{2K_1\cos(\sigma_a - \varphi)} \tag{55c}$$

The parameter σ_a therefore contains the ratio of rotational to translational motion (λ) or the location of the impact on the projectile. The parameter σ_b describes the direction and A the magnitude of the initial disturbance.

Additional Disturbance Due to Sabot Separation

The sabot separation is an additional impulse-generated disturbance that occurs at a distance s_s from the muzzle ($s = 0$). This generates the same kind of reaction as the muzzle jump, and the two solutions can simply be superimposed:

$$v(s) = 2A_m e^{ds}\cos(\omega s + \sigma_{am})\cos[-(1-\epsilon)\Phi + \sigma_{bm}] + 2A_s e^{ds_2}\cos(\omega s_2 + \sigma_{as})\cos[-(1-\epsilon)\Phi_2 + \sigma_{bs}] \tag{56a}$$

$$w(s) = -2A_m e^{ds}\cos(\omega s + \sigma_{am})\sin[-(1-\epsilon)\Phi + \sigma_{bm}] - 2A_s e^{ds_2}\cos(\omega s_2 + \sigma_{as})\sin[-(1-\epsilon)\Phi_2 + \sigma_{bs}] \tag{56b}$$

where

$$s_2 = s - s_s \quad \text{and} \quad \Phi_2 = \Phi - \Phi(s_s) \tag{57}$$

Similar expressions hold for the variables q, r, Θ, Ψ, y_g, and z_g. The parameters A_s, σ_{as}, σ_{bs} are determined by the disturbances due to sabot separation (v_s, w_s, q_s, and r_s) in the same way as for the muzzle jump [Eqs. (55)].

Implementation for Parameter Estimation

A maximum-likelihood cost function and a nongradient optimization method[12] are applied to determine the projectile parameters. The corresponding Fortran code runs on a PC and allows two kinds of evaluation:

1) *Velocity decrease and roll characteristics.* If there are test data for the decrease in velocity and for the roll angles, both can be evaluated either separately or together in one step using Eqs. (11) and (17). Then the characteristic static and dynamic aerodynamic coefficients, namely drag coefficient, rolling moment, and roll damping coefficient, can be estimated.

2) *Yawing characteristics.* The yawing characteristics can be evaluated either by using the measured pitch and yaw angles only or by adding the information from the measured deviations from the flight path. This allows one to estimate the pitching moment and thus the yawing length as well as the initial disturbances due to muzzle jump and sabot separation.

Due to the underlying analytical closed-form solutions, the results can be extrapolated to the muzzle or to greater distances. This makes it possible to use singular data even at great distances and to visualize the damping behavior once the aerodynamic characteristics have been estimated.

Results

A series of ten shots is used to demonstrate the evaluation of yaw-card data. Yawing lengths (equivalent to pitching-moment coefficients) and initial disturbances due to muzzle jump and sabot separation are estimated from the measured angles and dispersions using input data from Table 2.

Figure 5 shows the match in pitch and yaw angle vs arc length (range) for shots 1 and 9. It can be seen from the figure that the flight data of shot 9 are scattered more than the ones of shot 1. The mathematical model shows a very good approximation in the range of the experiments.

In Fig. 6 the angle of pitch is plotted vs the angle of yaw for shots 1 and 9. There are characteristic differences between the two results. In the case of shot 1, the jump due to sabot separation is almost perpendicular to the direction of yawing motion caused by

Table 2 Data for parameter estimation example

Quantity	Value	Status
Air density	1.2250 kg/m^3	Fixed
Projectile mass	5 kg	Fixed
Reference length	0.03 m	Fixed
Lateral moment of inertia	0.15 kg-m^2	Fixed
Longitudinal moment of inertia	0.00056 kg-m^2	Fixed
Initial flight velocity	1700 m/s	Fixed
Initial roll rate	0 Hz	Fixed
Drag coefficient	0.50000	Fixed
Rolling-moment coefficient	0.04	Fixed
Roll damping coefficient	−60	Fixed
Normal-force derivative	−15/rad	Fixed
Pitching-moment derivative	−70/rad	Variable
Pitch damping	−2000	Fixed
Value of muzzle jump	2 Hz	Variable
Angle of muzzle jump	0 deg	Variable
Value of sabot jump	2 Hz	Variable
Angle of sabot jump	0 deg	Variable
Initial angle of yaw	0 deg	Fixed
Initial angle of pitch	0 deg	Fixed
Initial y dispersion	0 cm	Fixed
Initial z dispersion	0 cm	Fixed
Location of sabot separation	8 m from muzzle	Fixed
Number of shots:	10	
Number of yaw cards per shot:	13 (14)	

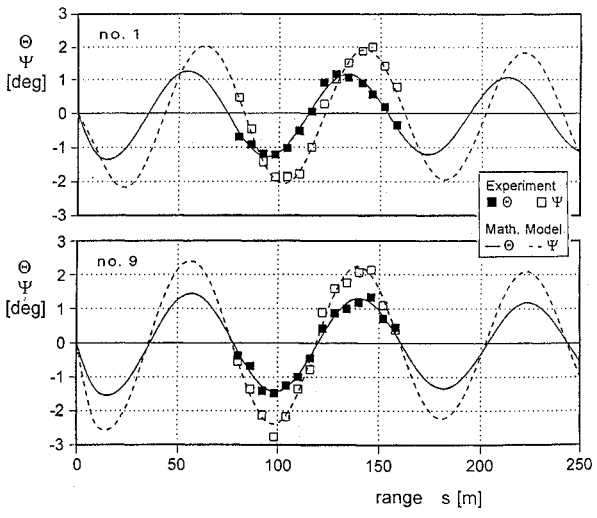

Fig. 5 Pitch and yaw angle vs range (shots 1 and 9).

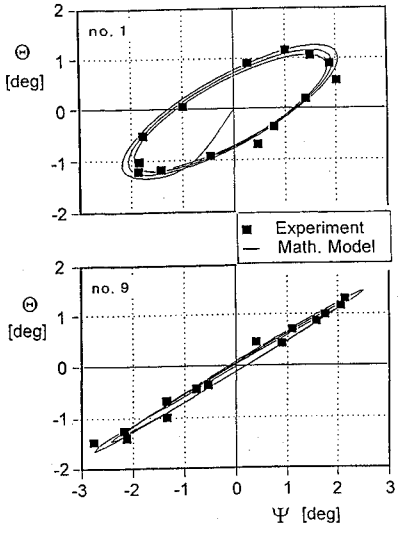

Fig. 6 Pitch angle vs yaw angle (shots 1 and 9).

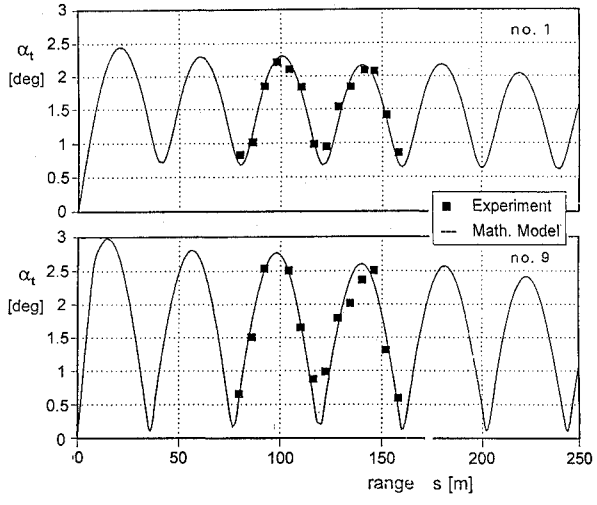

Fig. 7 Effective angle of attack vs range (shots 1 and 9).

the muzzle jump. This results in a widening of the yawing ellipsoid. Shot 9 on the contrary shows an almost ideal yawing motion behavior. In both shots the yawing ellipsoid turns slowly because of the rolling motion of the KE rod. Corresponding to the flight-path inclination, the center of the ellipsoid tends toward negative values of the pitch angle.

In Fig. 7 these different yawing characteristics are studied with regard to the effective angle of attack. The minimum effective angle of attack of shot 1 remains greater than 0.6 deg, whereas in the case of shot 9 it decreases almost to zero. Again the differences between the measured data and the identified fits for shot 9 are not as good as in the case of shot 1, but are still small.

Figure 8 shows the estimated pitching-moment derivatives for all ten shots under investigation. Seven results lie between -71/rad and -74/rad. This corresponds to a difference of less than 0.2 calibers in the estimation of the center of pressure, or less than 6 mm in physical coordinates, which indeed is an astonishingly good result for a yaw-card evaluation.

The remaining three shots show somewhat larger or smaller $C_{m\alpha}$ values, namely shots 3 (-76.5/rad), 5 (-70.3/rad), and 9 (-65.8/rad). From Fig. 9 it can be seen that these three shots contain large scatter in the experimental data. From the behavior of long KE rods it is known that strong transverse oscillations can be excited with frequencies much larger than the yawing frequency. Therefore, the quality of the identified results in such a case may be rather poor, because the mathematical model does not account for this structural mode.

The results of the evaluation of the initial muzzle jump are given in Fig. 10. The muzzle jump is characterized by its initial pitch

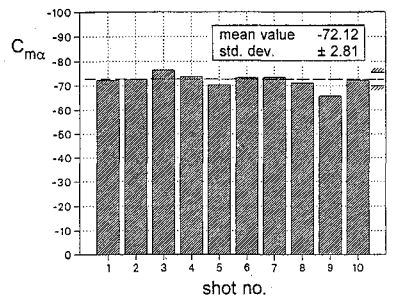

Fig. 8 Estimated pitching-moment derivatives (10 shots).

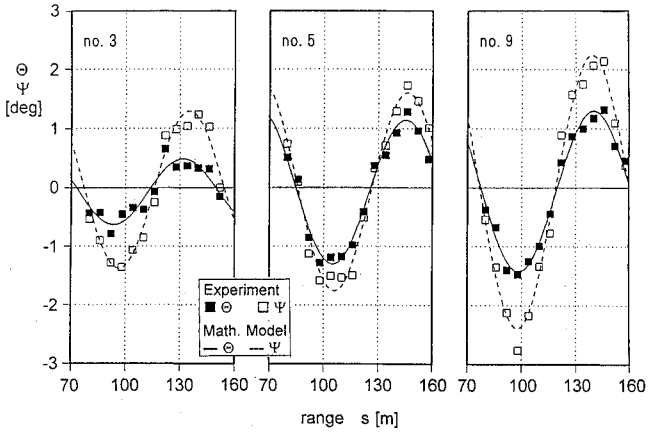

Fig. 9 Shots 3, 5, and 9: scatter of experimental data (pitch and yaw angles vs range).

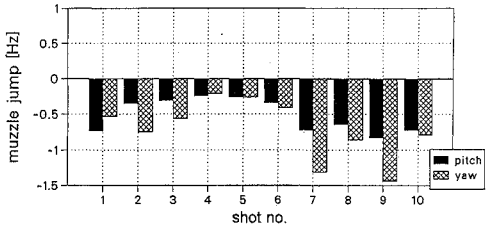

Fig. 10 Estimation of muzzle jump (10 shots).

Fig. 11 Estimation of jump due to sabot separation (10 shots).

rate and yaw rate, respectively. All the shots have a negative initial pitch rate (nose down) and yaw rate (nose left, seen from behind), which corresponds to the reverse motion of the barrel. So the motion of the barrel-projectile system can be identified qualitatively and quantitatively.

The jump due to sabot separation, Fig. 11, shows completely different behavior. The disturbance now acts in an arbitrary direction. The value of the jump due to sabot separation may be of the same order of magnitude as the muzzle jump. Therefore, it is essential to point out that this second disturbance must not be omitted in the general discussion of test results: an idealized sabot will produce no disturbance at all, but in reality there are disturbances. One goal of an improved design of projectiles must be the reduction of the disturbances due to sabot separation.

As discussed previously, shot 9 shows an unusually large pitching-moment derivative, which can be explained by structural oscillations. From Figs. 10 and 11 it follows that this shot suffers the

strongest muzzle jump of all trials. The same holds for the jump due to sabot separation, which acts in the reverse direction. In combination this leads to an extremely large excitation of the structural oscillation, which can be observed in the yaw- and pitch-angle characteristics.

In addition other quantities can be evaluated and discussed, such as roll characteristics or pitch damping. Moreover, a flight-path reconstruction on the basis of the measured dispersion data can be performed and may even be used to improve the results or to evaluate the observed experimental dispersion in detail.

Conclusions

Based on an analytical solution of the 6-DOF equations of motion, a parameter estimation method for projectiles was developed, which proved to be very effective. The method was introduced as a standard tool for the aeroballistic evaluations at Rheinmetall Company. Its application to the experimental data improved the quality of the interpretation of field tests considerably.

So far, the method does not handle nonlinear aerodynamic effects. It also does not include the influence of structural oscillations, which are observed for KE rods and need to be considered next.

Acknowledgment

The authors would like to thank E. A. Bockemüller, who developed[13] the analytical solution of the equations of motion for the case $I_x = 0$ and also gave advice, after his retirement from DLR, how to solve the case $I_x \neq 0$.

References

[1]Canning, T. N., Seiff, A., and James, C. S. (eds.), "Ballistic Range Technology," AGARD AG-138-70, Aug. 1970.

[2]Daniel, D. C., Winchenbach, G. L., and Browell, E. V., "The USAF Aeroballistic Research Facility," *24th Aeroballistic Range Assoc. Meeting*, 1973.

[3]Murphy, C. H., "Angular Motion of Spinning Almost Symmetric Missiles," Ballistic Research Lab., Tech. Rept. ARBRL-TR-02121, Nov. 1978.

[4]Whyte, R. H., and Hathaway, W. H., "Aeroballistic Range Data Reduction Technique Utilizing Numerical Integration," Tech. Rept. AFATL-TR-74-41, Eglin AFB, FL, Feb. 1974.

[5]Whyte, R. H., Jeung, A., and Bradley, J. W., "Chapman-Kirk Reduction of Free-Flight Range Data to Obtain Nonlinear Aerodynamic Coefficients," Ballistic Research Lab., Rept. BRL-MR-2298, AD-762148, May 1973.

[6]Hamel, P. G., "Determination of Aircraft Dynamic Stability and Control Parameters from Flight Testing," Paper 10, AGARD Rept. LS-114, May 1981.

[7]Jategaonkar, R. V., and Plaetschke, E., "Maximum Likelihood Parameter Estimation from Flight Test Data for General Non-linear Systems," DFVLR Rept. FB 83-14, March 1983.

[8]Jategaonkar, R. V., and Plaetschke, E., "Non-linear Parameter Estimation from Flight Test Data Using Minimum Search Methods," DFVLR Rept. FB 83-15, March 1983.

[9]Doherr, K.-F., Lehmann, G., and Schilling, H., "Identification of Stability and Control Parameters of a Brillant Ammunition," Paper 19, AGARD Rept. CP-451, May 1988.

[10]N. N., "Rotorcraft System Identification," AGARD Rept. AR-280, Oct. 1991.

[11]Weiss, S., Plaetschke, E., Rohlf, D., and Galleithner, H., "System Identification for X-31A Project Support—Lessons Learned So Far," Paper 14, AGARD Rept. CP-519, Oct. 1992.

[12]Jacob, H. G., "An Engineering Optimization Method with Application to STOL Aircraft Approach and Landing Trajectories," NASA TN D 6978, 1972.

[13]Bockemüller, E. A., and Weiss, S., "Analytische Lösung der wegabhängigen Bewegungsgleichungen von schlanken rotierenden Geschossen," DLR Inst. für Flugmechanik, Braunschweig, DLR Rept. IB 111-90/35, Aug. 1990.

[14]Larrabee, E. E., "Aerodynamic Penetration and Radius as Unifying Concepts in Flight Mechanics," AIAA Paper 66-16, Jan. 1966; see also *Journal of Aircraft*, Vol. 4, No. 1, 1967, pp. 28–35.

[15]Uffelmann, F. L., "The Initial Disturbances Affecting the Direction of Trajectory of a Shot Fired from a High-Velocity Gun," *Proceedings of the Royal Society of London, Series A: Mathematical and Physical Sciences*, Vol. 272, 1963, pp. 331–362.

[16]Glotz, G., "Investigation of the Stability of the Flow during the Sabot Discard," Process. Symp. Ball., Orlando, FL, 1981.

[17]Schmidt, E. M., and Plostins, P., "Aerodynamics of Asymmetric Sabot Discard," AIAA Paper 82-1301, Aug. 1982.

[18]Bornstein, J., Celmins, I., Plostins, P., and Schmidt, E., "Launch Dynamics of Fin-Stabilized Projectiles," *Journal of Spacecraft and Rockets*, Vol. 29, No. 3, 1992, pp. 166–172.